Linking near-surface and satellite remote sensing measurements of deciduous broadleaf forest phenology

Koen Hufkens [a,*], Mark Friedl [a], Oliver Sonnentag [c], Bobby H. Braswell [d],
Thomas Milliman [d], Andrew D. Richardson [b]

[a] Department of Geography and Environment, Center for Remote Sensing, Boston University, Boston, Massachusetts, USA
[b] Department of Organismic and Evolutionary Biology, Harvard University, Cambridge, Massachusetts, USA
[c] Département de Géographie, Université de Montréal, Montreal, Canada
[d] University of New Hampshire, Complex Systems Research Center, Durham, New Hampshire, USA

ARTICLE INFO

ABSTRACT

Green leaf phenology is known to be sensitive to climate variation. Phenology is also important because it exerts significant control on terrestrial carbon cycling and sequestration. High-quality measurements of green leaf phenology are therefore increasingly important for understanding the effects of climate change on ecosystem function and biosphere–atmosphere interactions. In this paper, we compare "near-surface" and satellite remote sensing-based observations of vegetation phenology at four deciduous forest sites. Specifically, we addressed three questions related to how observations of plant phenology measured by red–green–blue (RGB) cameras mounted on towers above forest canopies are related to measurements of phenology acquired by moderate resolution sensors on satellites. First, how are estimated phenophase transition dates — or the observable stages in the life cycle of plants — influenced by the choice of vegetation index (VI) measured by remote sensing? Second, are VIs and phenological metrics derived from near-surface and satellite remote sensing comparable, and what is the nature and magnitude of covariation between near-surface and satellite-remote sensing-based estimates of phenology at seasonal and interannual time scales? Third, does near-surface remote sensing data provide a basis for validating satellite-derived land surface phenology products and what are the requirements for achieving this goal? Our study provides substantial support for future efforts linking satellite and near-surface remote sensing. We show significant agreement between phenological time series and metrics derived from these two data sources. However, issues of scale and representation strongly influence the relationship between near surface and satellite remote sensing measures of phenology. In particular, intra- and interannual correlation between time series from each source are dependent on how representative the camera FOV is of the regional landscape. Further, our results show that the specific VI used to monitor phenology exerts substantial influence on satellite VI derived phenological metrics, and by extension, how they compare to VI time series and metrics obtained from near-surface remote sensing. These results improve understanding of how near-surface and satellite remote sensing complement each other. However, more work is required to develop formal protocols for evaluating, calibrating and validating satellite remote sensing phenology products using near surface remote sensing at a regional to continental scale.

© 2011 Elsevier Inc. All rights reserved.

1. Introduction

Green leaf phenology, the study of seasonal leaf development, senescence and abscission, is known to be an indicator of climate change (Cleland et al., 2007; Kemp, 1983; Menzel et al., 2006; Parmesan, 2007). In particular, phenology in temperate ecosystems is strongly linked to seasonality in solar radiation (photoperiod) and temperature and is therefore an effective integrator of weather at weekly to seasonal time scales (Schwartz et al., 2006). As a consequence, climate change at mid and high-latitudes is affecting the phenology of temperate and boreal ecosystems, and current estimates suggest that spring phenology has advanced by as much as two days per decade over the last half-century (Parmesan & Yohe, 2003). While some studies have noted heterogeneous responses to climate warming (Zhang et al., 2007), most phenological assessments based on remote sensing (Myneni et al., 1997; Bogaert et al., 2002), field observations (Sparks & Menzel, 2002) or atmospheric CO_2 measurements (Keeling et al., 1996), suggest an earlier spring

* Corresponding author. Tel.: +1 617 353 8846.
E-mail address: koen.hufkens@gmail.com (K. Hufkens).

onset and longer growing season overall (Badeck et al., 2004; Penuelas et al., 2002).

Changes in phenology have important implications for ecosystem function and biosphere–atmosphere interactions. Year-to-year variability in gross primary production and ecosystem respiration are influenced by inter-annual variations in temperature. As a result, variation in phenology exerts significant influence on carbon cycling and sequestration (e.g. Richardson et al., 2009, 2010). Similarly, spatial patterns in forest gross primary production correlate strongly with growing season length (Baldocchi et al., 2005; Churkina et al., 2005; Nemani et al., 2003). Finally, because changes in canopy properties affect surface meteorology, vegetation phenology also influences atmospheric boundary layer properties and dynamics (Hollinger et al., 1999; Sakai et al., 1997). Thus, high-quality measurements of green leaf phenology at landscape-scales are important for a diverse array of questions related to the effects of climate change on ecosystem function and biosphere–atmosphere interactions.

Phenological events have been documented for centuries in Europe and Japan by hobbyists, generations of the same family, and even by communal decree (Chuine et al., 2004; Fitter & Fitter, 2002; Sparks & Menzel, 2002). These historical records document phenophase dates (the observable stages in the life cycle of a plant or animals for important phenological events such as leaf-out, flowering, or harvest), and have provided insight into long-term climate trends (Sparks & Menzel, 2002). Recently, a number of initiatives including the USA National Phenology Network (USA-NPN, Betancourt et al., 2007), the "Global Learning and Observations to Benefit the Environment" (GLOBE) science network, and the French "Réseau National de suivi à long terme des ECOsystèmes FORestiers" (RENECO-FOR) network have attempted to expand and extend these records. However, data collected through these efforts are constrained by one or more factors including limits to species ranges, local or regional spatial extent, inconsistencies in observations among observers, or low observation frequency (Chuine et al., 2000; Menzel, 2002). High temporal frequency observations of vegetation phenology, such as measurements obtained from above- and below-canopy radiometric instruments provide detailed information related to the phenology of forest canopies based on measurable biophysical quantities (e.g., f_{APAR}; Jenkins et al., 2007). However, measurements collected in this fashion are influenced by spatial heterogeneity, and as a result, adequate sampling of landscape-scale phenological dynamics is difficult.

Recently, near-surface remote sensing using conventional or networked red–green–blue (RGB) cameras has been shown to provide a cost effective way to monitor green leaf phenology (Graham et al., 2009, 2010; Jacobs et al., 2009; Richardson et al., 2007, 2009). In particular, data retrieved from RGB cameras have been used to monitor vegetation development and canopy CO_2 fluxes (Ahrends et al., 2009; Richardson et al., 2007, 2009). A key advantage of near-surface remote sensing is that it allows phenological dynamics to be monitored at high temporal frequency and over broader spatial extents relative to visual observations or above- and -below canopy radiometric measurements (Wingate et al., 2008). Indeed, the measurement scale of RGB cameras, which can vary from that of individual trees to entire landscapes, opens new possibilities for bridging the gap between ground and satellite-based phenology measurements (Morisette et al., 2008; Richardson et al., 2007). While numerous studies have explored the use of satellite remote sensing data for monitoring terrestrial phenology at landscape to regional scales (Fisher et al., 2007; Myneni et al., 1997; Soudani et al., 2008; White et al., 2009), assessing the relationship between ground- and satellite-based measurements of phenology remains a challenge. Moreover, no study has previously attempted to carefully analyze the relationship of near-surface remote sensing of canopy phenology to corresponding measurements from satellite remote sensing.

In this paper, we present results from a study in which we compare near-surface and satellite remote sensing-based observations of vegetation phenology. Given the demonstrated utility of both sources of information related to phenology, we address several outstanding questions related to how observations of plant phenology scale from the spatial resolution of individual plants and leaves measured by RGB cameras to the landscape resolution measured by satellite sensors. Specifically, we address three main questions:

(1) How are estimated phenophase dates influenced by the choice of vegetation indices (VIs) measured by remote sensing?
(2) Are VIs and phenological metrics derived from near-surface and satellite remote sensing comparable, and what is the nature and magnitude of covariation between near-surface and satellite-remote sensing-based estimates of phenology at seasonal and interannual time scales? and
(3) Does near-surface remote sensing data provide a basis for validating satellite-derived land surface phenology products and what are the requirements for achieving this goal?

2. Materials and methods

2.1. Near-surface remote sensing site selection

Near-surface remote sensing data was acquired from the Pheno-Cam data repository (Richardson et al., 2007: http://phenocam.sr.unh.edu). This repository includes time series of RGB camera imagery from more than 50 sites distributed across North America. Not all RGB cameras within the repository are directly internet-connected. However, for consistency we will refer to all RGB cameras as webcams. To support a careful and detailed analysis of the relationship between satellite and near-surface data sets, we limited the number of sites used in this study. Specifically, we selected sites based on two main criteria: (1) the length of the available time series, and (2) qualitative assessment of the quality of the available time series. Further, to ensure that selected sites had strong seasonal phenology, only deciduous broadleaf forest sites were considered. After careful assessment of imagery in the PhenoCam data repository we selected four sites for inter-comparison. These sites included the Bartlett Experimental Forest (44.06° N, 71.29° W, elev. 268 m asl.) located within the White Mountain National Forest, Smoky Look in the Great Smoky Mountains National Park (35.63° N, 83.94° W, elev. 739 m asl.), the Green River valley in Mammoth Cave National Park (37.19° N, 86.10° W, elev. 226 m asl.) and the Dolly Sods Wilderness area in the Monongahela National Forest (39.11° N, 79.43° W, elev. 1141 m asl.). The Bartlett camera was installed specifically for phenological observations; the latter three cameras were installed by federal agencies for air quality monitoring.

Each of the cameras was installed using different configurations. The camera located at Bartlett Experimental Forest is directed towards the north inclined downward at 15° from the horizontal. The field of view (FOV) of this camera is dominated by northern hardwood tree species (American beech, *Fagus grandifolia*; Sugar maple, *Acer saccharum* and yellow birch, *Betula alleghaniensis*). The cameras at Great Smoky National Park and the Dolly Sods Wilderness Area are directed toward (and approximately leveled with) the eastern and southern horizons, respectively, and both FOVs are dominated by northern hardwood tree species (American beech, *F. grandifolia*; Sugar maple, *A. saccharum* and yellow birch, *B. alleghaniensis*). The camera at Mammoth Cave National park points north–northwest and downward from the horizon, with Oak–Hickory forest (*Quercus* sp., *Carya* sp.) dominating the FOV. An overview of the sites and their characteristics is given in Table 1. To characterize spatial heterogeneity of land cover within and between MODIS pixels at each site, we used the Multi-Resolution Land Characteristics Consortium 2006 National Land Cover Database (NLDC, Fry et al., 2011).

Table 1
Summary of PhenoCam site characteristics, including geographic location, camera type, source of data, time-span analyzed, and predominant vegetation type in the field of view (FOV).

Site	Location (latitude, longitude in decimal degrees)	Elevation (m)	Direction of FOV	Camera Type	Data source	Years	Vegetation type
Bartlett Experimental Forest	44.06, −71.29	268	N	Axis211	PhenoCam network	2006–2010	Northern Hardwood Forest
Air quality camera, Dolly Sods National Park	39.11, −79.43	1141	S	Olympus D-360L	US Forest Service	2004–2010	Northern Hardwood/ Red Spruce Forest
Air quality camera, Mammoth Cave National Park	37.19, −86.10	226	NNW	Olympus D-360L	National Park Service	2002–2010	Oak, Hickory Forest
Air quality camera, Great Smoky National Park	35.63, −83.94	793	E	Olympus D-360L	National Park Service	2000–2010	Northern Hardwood Forest

2.2. Data sets

2.2.1. Near-surface remote sensing image acquisition and pre-processing

For each of the selected sites all available images were downloaded from the PhenoCam server. Because webcam images include a mix of landscape, sky, and other features, images were manually segmented and data were extracted for user-selected regions of interest (ROI) within each webcam FOV (Fig. 1). Each ROI was selected to provide high quality data representative of dominant vegetation types in the scene. To this end, we attempted to select ROIs covering multiple tree canopies located in the foreground of each image. Furthermore, selection of a ROI located in the foreground minimizes weather effects such as fog and clouds which could negatively influence the quality of phenological information that can be obtained from webcams (Richardson et al., 2009).

Using digital number values for the red, green, and blue color planes from each image, we calculated the average excess green index (ExG$_W$) for each ROI. The excess green index has been previously used in agriculture to discriminate leaf cover from soil background (Woebbecke et al., 1995), and Richardson et al. (2009) recently demonstrated its utility for monitoring forest canopy phenology. This index is defined as:

$$ExG_w = 2 * G - (R + B); \tag{1}$$

where R, G, and B the digital numbers of the red, green and blue channels in the ROI.

Each of the cameras acquired multiple images for each day at different time intervals. Unlike previous studies (Ahrends et al., 2008a,b; Richardson et al., 2009), we did not estimate daily values using average midday images. Instead, moving-windows were used to calculate the quantile for each ExG$_W$ value using a window size of three days. The 90th percentile ExG$_W$ value for each 3-day period was then used to produce time series with 3 day time steps for
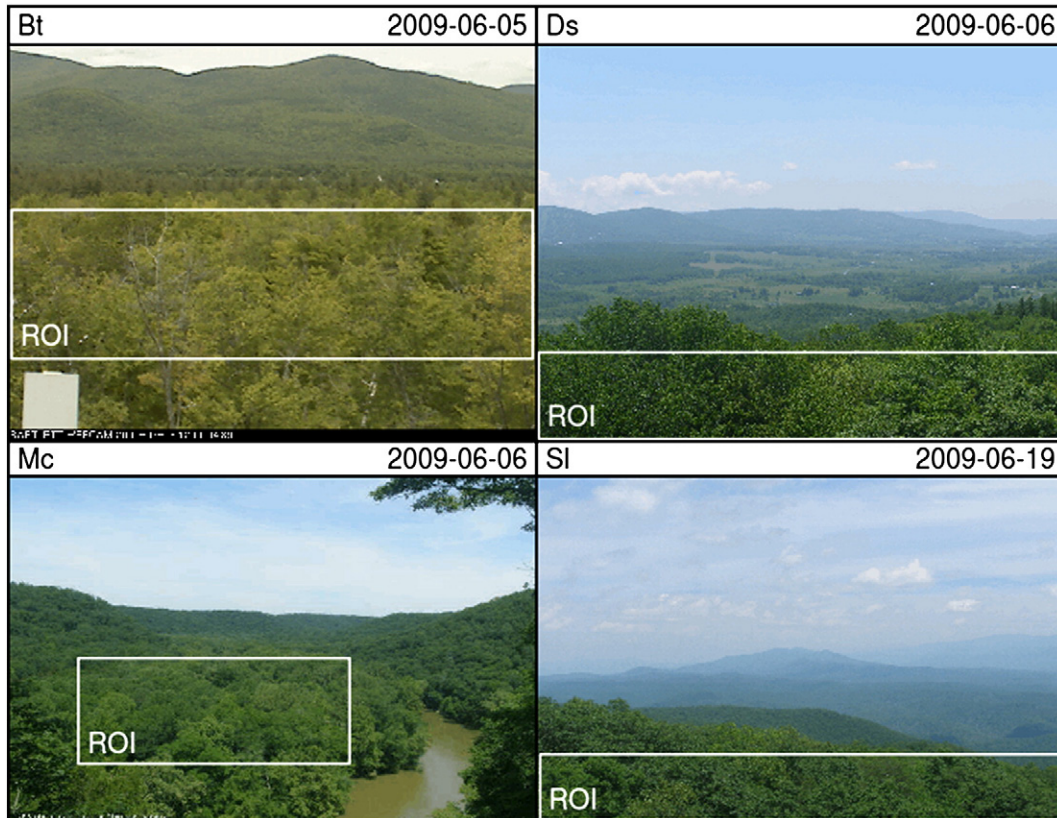

Fig. 1. Digital camera field of view and regions of interests (ROI) at each of the four sites (Bartlett Experimental Forest, Bt; Look Rock in Smoky Look National Park, Sl; Mammoth Cave National Park, Mc and Dolly Sods Wilderness, Ds).

each camera. This approach reduces day-to-day variability caused by changing weather and illumination conditions (Sonnentag et al., 2012).

2.2.2. Satellite remote sensing image acquisition and preprocessing

MODIS surface reflectance data were acquired for pixels corresponding to the geographic location and duration of each near-surface time series. MODIS data was downloaded from the Oak Ridge National Laboratory Distributed Active Archive Center (http://daac.ornl.gov/) for 5×5 pixel (~2.3×2.3 km) regions centered over the location of each camera site (Table 1, column 2). All data used for this analysis were based on the most recently available version of MODIS land products (so-called Collection 5). For each pixel we extracted: (1) 8-day MODIS nadir BRDF-adjusted surface reflectance data values for MODIS bands one to four (and associated quality assurance data), (2) MODIS Land Cover Type data, and (3) MODIS Land Cover Dynamics (hereafter, MODIS phenology) data (Friedl et al., 2010; Ganguly et al., 2010; Schaaf et al., 2002). MODIS reflectance data that were contaminated by snow, classified as water, urban, barren or snow/ice, or that were flagged as missing (e.g., due

to clouds) were removed. The remaining pixels were averaged and used to calculate three VIs:

(1) the Enhanced Vegetation Index (EVI; Huete et al., 2002):

$$EVI = G * \frac{NIR - RED}{NIR + C1 * RED - C2 * BLUE + L};$$ (2)

(2) the Normalized Difference Vegetation Index (NDVI; Tucker, 1979):

$$NDVI = \frac{NIR - RED}{NIR + RED};$$ (3)

and (3) the Excess Green Index (ExG_M):

$$ExG_M = 2 * GREEN - (RED + BLUE);$$ (4)

where *RED*, *GREEN*, *BLUE*, and *NIR* correspond to MODIS band 1 (620–670 nm), band 4 (545–565 nm), band 3 (459–479 nm),
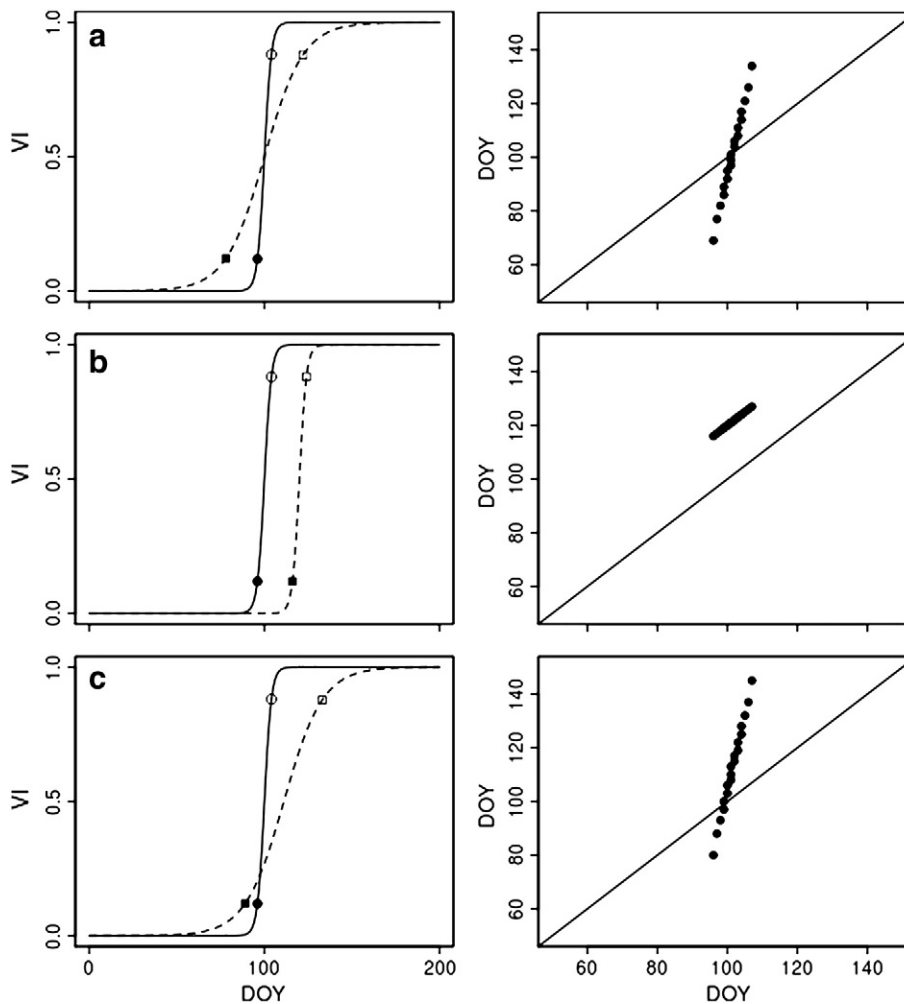

Fig. 2. a–c. Schematics showing biases of modeled versus actual VI dynamics during spring using logistic models. The black lines show reference logistic models, and the dashed lines illustrate the effects of changes in logistic function parameters for (a) a change in steepness but no change in the phase in the logistic curve, (b) a change in the phase of the curve but no change in the overall steepness, (c) a change in both steepness and phase. Phenological metrics indicating the timing of greenness onset and maximum based on the logistic fits are denoted with closed and open circles and squares, respectively. Panels on the right display the phenological metrics as 5 percent intervals of the total amplitude comparing the results for the solid (x-axis) to the solid line (y-axis).

and band 2 (841–871 nm); and *L*, *C*1, *C*2 are aerosol resistance co-efficients (equal to 1, 6, 7.5, respectively); and *G* is a gain factor (=2.5) (Huete et al., 2002). Note that the ExG_M index was included to provide the most direct comparison between MODIS and the camera data. Example time series of the MODIS VI's for all sites are shown in Fig. 2.

2.3. Estimating and comparing phenological metrics

2.3.1. Logistic model fits

Following an approach that is widely used in the phenology scientific community (Fisher et al., 2006, 2007; Richardson et al., 2006, 2009; Schwartz & Hanes, 2010; Zhang et al., 2003), we used a logistic
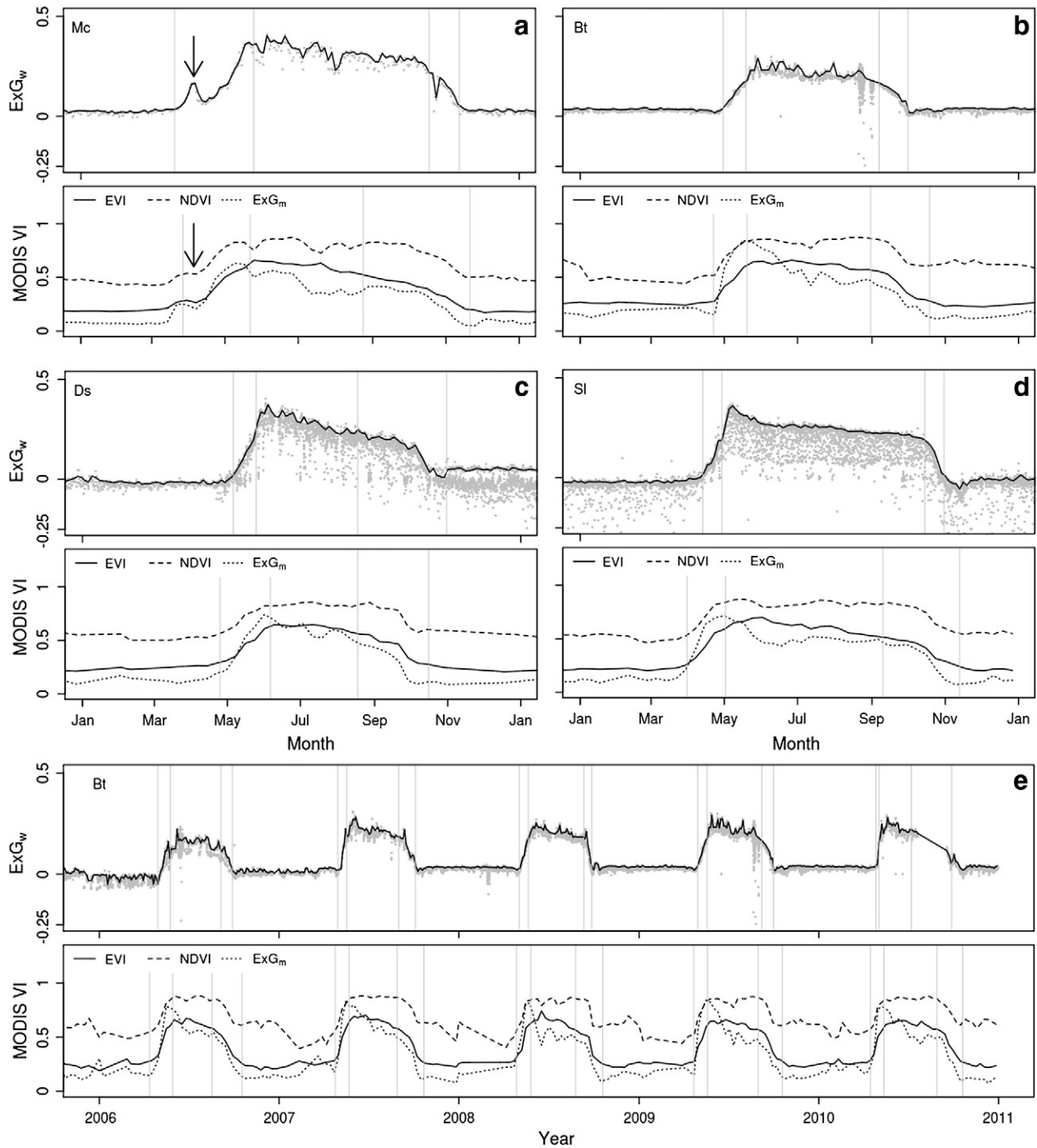

Fig. 3. Overview of different dynamics displayed by the various VIs at each the four sites of interest (a: Mammoth Cave National Park, Mc; b: Bartlett Experimental Forest, Bt; c: Look Rock in Smoky Look National Park, Sl; and d: Dolly Sods Wilderness, Ds. and e: an overview of the complete Bartlett Experimental Forest time series. The top panels show the unprocessed raw excess green digital camera data (ExG_W, gray dots) and processed data after applying the moving window quantile approach (black line). The bottom panels show the enhanced vegetation index (EVI, black line), the normalized difference vegetation index (NDVI, dashed line) and excess green (ExG_M, dotted line) from MODIS. The full gray vertical lines, from left to right, denote the timing of greenness onset, maximum, decrease and minimum (G_{in}, G_{max}, G_{dec}, G_{min}) for the smoothed ExG_W and MODIS EVI data, respectively. The black arrow in panel a) indicates early onset of the growing season and subsequent die-back due to a severe spring frost in 2007.

equation to model spring and autumn dynamics in webcam and MODIS-derived VIs as a function of time:

$$VI(t) = a + \frac{b}{1 + e^{(c-d*t)}};\tag{5}$$

where t is time (in days), c and d are coefficients that determine the timing and speed of canopy development (or senescence), respectively, and a and b control the lower and upper limits of the function, respectively. For this work, we estimate values for b, c and d by non-linear least squares fits to the data, and a is assigned the median VI value during the first and last two months of the time series (i.e., during the winter, dormant phases). The logistic equation presented above was fit separately to spring and autumn webcam and MODIS VI time series at each site, with parameters optimized separately for each year of data. To model spring dynamics we used data spanning day of year (DOY) 1–185. For autumn dynamics, we used data from DOY 185–365.

Using this framework, we estimated DOY phenophase transition dates (hereafter, phenological metrics) using the method described by Zhang et al. (2003). Phenological metrics considered here include the dates of onset for VI increase, VI maximum, VI decrease, and VI minimum (hereafter G_{in}, G_{max}, G_{dec} and G_{min} respectively, see Fig. 3a). Further, the duration of greenup ($G_{max}-G_{in}$) and senescence ($G_{min}-G_{dec}$) periods were calculated, which provide information about the speed at which leaves develop during spring and senescence during autumn. We also recorded the DOY at 5 percent intervals between 5 and 95% of the amplitude for each estimated logistic fit. These metrics were used to compare characteristics of models fitted to data from the webcams with those fitted to MODIS data. Finally, for each of the sites we retrieved values for corresponding phenological metrics from the MODIS phenology product (Ganguly et al., 2010). Although the procedure described above is similar to the algorithm used in the MODIS product generation, different methods were used to pre-process the webcam RGB digital number data and MODIS surface reflectance data (specifically, to fill gaps and remove noise). As a result, some differences between the phenological metrics estimated in this work and those from MODIS and the standard NASA product arise from differences in pre-processing. However, these differences should be modest. A full description of the MODIS phenology algorithm and product is provided by Zhang et al. (2006) and Ganguly et al. (2010).

2.3.2. Comparing near-surface and satellite-based remote sensing phenological metrics

To quantify the logistic model fit, we report the root mean squared error (RMSE) and the coefficient of variation (CV) separately for the spring and autumn for each site. Mean and standard deviations for phenological transition dates (G_{in}, G_{max}, G_{dec} and G_{min}), and greenup and senescence durations were also calculated for each site and year. These metrics provide information about relationships among phenophase transition dates derived from the different data sources and VIs. In this context, it is important to note that variance in phenological indicators across years reflects inter-annual variation in the estimated phenological metrics. We also calculate the mean absolute error (MAE) between the ExG$_W$ and MODIS VI-based phenological metrics. Finally, Spearman rank correlations (Spearman, 1904) were used to quantify covariation across years between the ExG$_W$ and MODIS VI based metrics. This test provides a non-parametric way to quantify how two measurements covary. Correlation values were considered significant for $p<0.05$.

As part of our analysis we also assess the logistic fits for biases in either phase (d) or slope (c). To do this, we identify three scenarios in which phenological dynamics during greenup and senescence measured by different sources might diverge from one another (Fig. 2). For the sake of illustration, we focus on spring phenology only. In the first case, models fit to different input data have the same phase, but different slopes or rates of change (Fig. 2a). In the second case, different models have similar rates of change, but their phase is different, thereby shifting the position of one curve relative to the other (Fig. 2b). Finally, in the third case, differences in both the slope and phase are present (Fig. 2c).

To summarize results from this analysis we computed an index we call the "*bias ratio*" (BR), which is designed to quantify the nature and magnitude of bias in logistic fits based on the satellite VIs relative to the logistic fits based on the ExG$_W$ data:

$$BR = \sum_{i=1}^{n} e_i/|e_i|;\tag{6}$$

where e_i is the deviation between the logistic fit for the satellite date relative to the webcam data, and n is 19, corresponding to 5 percent increments in the amplitude of each fit from 5 to 95%. The value of this metric indicates whether model fits to the satellite VIs are generally positively biased ($\sim$1), negatively biased (~-1) or display a more complex pattern including a change in steepness and bias ($\sim$0) relative to the ExG$_W$ data. A perfect agreement between logistic fits will result in a BR value of 0. To provide further insight into differences in phenological dynamics we plot the deviations between the satellite data and the webcam data at 5 percent increments.

3. Results

3.1. Near-surface and satellite remote sensing time series and phenological metrics

Day-to-day variability caused by changing weather and illumination conditions was reduced by the running quantile method and the resulting VI time series were relatively noise-free. To illustrate, Fig. 3 shows sample time series for each of the sites and an overview of the complete time series of Bartlett Forest (Fig. 3e). This figure shows both the raw data and the time series after removing day-to-day variability using the method described in Section 2.2. All of the time series display pronounced asymmetric seasonal phenology. Spring greenup is characterized by a rapid rise in ExG$_W$, while autumn dynamics are less abrupt and generally display more gradual change. In addition, and most notably at the Dolly Sods and Smoky Look sites, a pronounced peak is evident in ExG$_W$ early in the season before it levels off and becomes stable until the onset of senescence (Fig. 3c–d). Both of these sites display faster increase in ExG$_W$ during spring relative to more gradual rates of increase at both the Bartlett Forest and Mammoth Cave sites (Fig. 3a–b).

Removing MODIS reflectance data contaminated by snow, classified as water, urban, barren or snow/ice resulted in MODIS time-series that were relatively noise-free. However, distinct differences in the phenological dynamics represented by MODIS EVI, NDVI and ExG$_M$ time series are clearly evident (Fig. 3). Both the NDVI and ExG$_M$ show rapid increase and decrease during spring and autumn relative to more gradual dynamics evident in EVI values. Although not as pronounced as in the camera data, the ExG$_M$ data also exhibit a peak during late spring. Further, asymmetry between spring and autumn phenology noted in the ExG$_W$ data is also present in both the ExG$_M$ and EVI time series. The NDVI data, on the other hand, displays a more symmetric profile and the general shape is similar to a piecewise linear function characterized by uniform increase and decrease in VI values during spring and autumn, with relatively stable values during much of the growing season. In this context, it is important to note that land cover at each of the sites included a mixture of vegetation and land use, but was dominated by deciduous or mixed forest types (Fig. 4). As a result, some of the
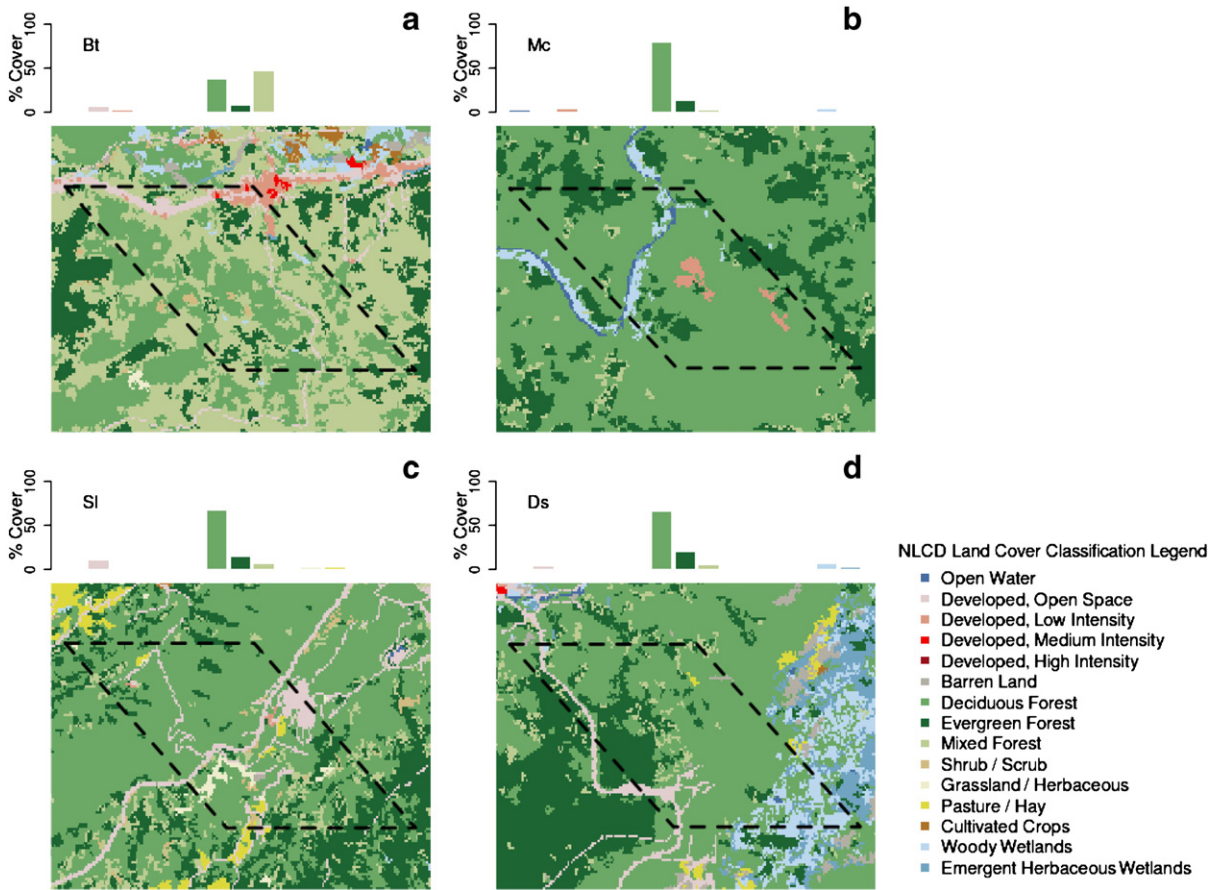
Fig. 4. An overview of the National Land Cover Database (NLCD) land cover heterogeneity within the 5×5 MODIS pixel windows, as marked by dashed black lines, surrounding the near-surface remote sensing camera sites for a: Bartlett Experimental Forest, Bt; b: Mammoth Cave National Park, Mc; c: Look Rock in Smoky Look National Park, Sl; and d: Dolly Sods Wilderness, Ds. The percentage land cover (%) is plotted as a color coded bar chart at the top of every panel.

differences between the webcam and MODIS time series likely arise from land cover heterogeneity within and across MODIS pixels at each site.

Inspection of statistical metrics for logistic fits to the different VIs shows that RMSEs are lowest for the ExG_w and MODIS VI based models (Table 2, top). Average RMSE values for MODIS VI data are slightly lower (0.009–0.007) than those for ExG_w data, with spring and autumn RMSE values of 0.018 and 0.016, respectively. Coefficients of variation, however, present a more balanced picture of the errors with very similar values across all VIs (Table 2, bottom).

Table 2
Root Mean Squared Error (RMSE) and the Coefficient of Variation (CV) across all sites for the logistic model fits. Values are reported separately for spring and fall data.

	Index	Spring	Fall
RMSE	ExG_W	0.018	0.016
	EVI	0.004	0.006
	NDVI	0.009	0.007
	ExG_M	0.014	0.008
	MCD12Q2	/	/
CV	ExG_W	0.455	0.358
	EVI	0.358	0.280
	NDVI	0.724	0.347
	ExG_M	0.343	0.219
	MCD12Q2	/	/

Visual interpretation of phenological dynamics in ExG_W and MODIS VI data are consistent with observed patterns in the estimated phenological metrics. However, comparison of metrics derived from the camera data with metrics derived from MODIS VIs reveal important patterns and differences. On average, values for the date of increase in ExG_W (G_{in}) are later relative to metrics based on EVI, NDVI and ExG_M data (Table 3); Similarly, the date of onset of maximum VI (G_{max}) is generally earlier for NDVI and ExG_M, and later for EVI and the MODIS phenology product values. Patterns among metrics derived from different VI time series in the autumn are consistent with those in spring, where ExG_W, NDVI and ExG_M show later onset of VI decrease, but earlier onset of VI minimum. In contrast, the slow rate of change in autumn MODIS EVI results in earlier estimates of the onset of VI decrease and later estimates for the onset of greenness minimum. This pattern is also present in the MODIS phenology product data.

Differences in estimated greenup and senescence periods are caused by systematic patterns in estimates of the timing of VI increase, maximum, decrease and minimum (Table 3). As a consequence, observed patterns in these quantities are generally consistent with patterns in the individual metrics described above. For example, the average greenup period from the ExG_W, NDVI and ExG_M for the Mammoth Cave site is 25, 23 and 15 days, respectively. In contrast, estimates based on EVI and the MCD12Q2 have periods of 32 and 43 days, respectively. A similar trend is present in the estimated senescence periods, where again, senescence is almost twice as long for EVI and the MODIS phenology product (77,

Table 3

Mean and standard deviation in day of year for phenological metrics: DOY for onset of greenness increase, maximum, decrease, minimum (G_{in}, G_{max}, G_{dec} and G_{min} respectively). In addition, mean and standard deviation in greenup and senescence periods are reported (in days). Results are reported for each of the four sites examined (Bartlett Experimental Forest, Bt; Look Rock in Smoky Look National Park, Sl; Mammoth Cave National Park, Mc and Dolly Sods Wilderness, Ds) and for both near-surface (ExG_W) and satellite based (EVI, NDVI and ExG_M) estimates including the MODIS MCD12Q2 product. Values are rounded to the nearest integer. N refers to number of years of data at each site.

Index		ExG_W		EVI		NDVI		ExG_M		MCD12Q2	
		Mean	Stdev	Mean	Stdev	Mean	Stdev	Mean	Stdev	Mean	Stdev
Bt	G_{in}	120	2	111	6	114	9	116	3	124	15
(N = 4)	G_{max}	137	9	143	7	135	7	125	7	156	2
	G_{dec}	237	27	239	5	255	8	248	6	223	5
	G_{min}	273	3	293	1	275	7	285	5	298	3
	Greenup	17	7	32	9	21	12	9	7	32	13
	Senescence	36	27	54	4	20	12	37	9	75	2
Sl	G_{in}	107	6	94	7	98	6	95	5	90	7
(N = 9)	G_{max}	126	8	129	7	117	6	107	7	142	8
	G_{dec}	288	15	250	5	282	6	276	9	221	6
	G_{min}	306	9	315	7	305	8	304	8	331	8
	Greenup	19	8	35	10	18	6	12	6	51	10
	Senescence	19	14	65	8	23	7	28	8	110	10
Mc	G_{in}	96	8	91	6	92	6	90	8	92	6
(N = 8)	G_{max}	121	15	123	9	115	9	105	9	135	8
	G_{dec}	261	25	235	9	274	8	269	11	204	8
	G_{min}	309	5	312	7	307	7	304	6	321	8
	Greenup	25	18	32	10	23	11	15	13	43	11
	Senescence	48	20	77	11	33	8	35	10	116	15
Ds	G_{in}	128	5	113	3	111	9	115	7	117	7
(N = 6)	G_{max}	142	6	156	12	152	7	142	6	169	7
	G_{dec}	241	23	225	10	255	11	234	12	220	7
	G_{min}	303	8	295	15	287	8	284	3	297	5
	Greenup	15	4	43	14	42	10	26	10	52	8
	Senescence	62	25	69	10	32	16	50	14	77	6

116 days) compared to estimates based on ExG_W, NDVI and ExG_M data (48, 33 and 35 days). This trend is observed across all sites, with average greenup and senescence periods that are consistently shorter for estimates based on ExG_W, ExG_M and NDVI data relative to those derived from MODIS EVI data and the MODIS phenology product.

To assess systematic biases among values based on different input data relative to the webcam data, we computed the mean

Table 4

Mean absolute error (MAE) and minimum and maximum values for the difference between the ExG_W and satellite based phenological indicators for: DOY of onset in greenness increase, maximum, decrease, minimum (G_{in}, G_{max}, G_{dec} and G_{min} respectively, in Doy). Mean and standard deviations for spring greenup and fall senescence periods are reported (in days). Data are provided for four different sites (Bartlett Experimental Forest, Bt; Look Rock in Smoky Look National Park, Sl; Mammoth Cave National Park, Mc and Dolly Sods Wilderness, Ds). Values are rounded to the nearest integer.

Index		Mean absolute error (min–max)							
		EVI		NDVI		ExG_M		MCD12Q2	
Bt	G_{in}	9	(5–17)	9	(5–13)	4	(1–11)	10	(3–27)
(N = 4)	G_{max}	5	(1–10)	4	(1–8)	12	(8–18)	16	(14–17)
	G_{dec}	11	(3–18)	8	(1–13)	3	(1–7)	26	(20–33)
	G_{min}	19	(17–22)	4	(0–7)	12	(7–15)	25	(22–28)
	Greenup	15	(9–22)	9	(4–16)	8	(6–17)	18	(13–21)
	Senescence	30	(20–39)	17	(1–50)	20	(11–49)	51	(42–60)
Sl	G_{in}	15	(12–24)	10	(4–18)	13	(6–23)	18	(13–27)
(N = 9)	G_{max}	4	(0–12)	10	(0–22)	20	(9–36)	15	(9–27)
	G_{dec}	38	(6–56)	12	(1–30)	12	(0–29)	67	(28–88)
	G_{min}	9	(0–15)	3	(0–11)	5	(1–8)	24	(16–34)
	Greenup	19	(9–29)	4	(1–13)	10	(2–23)	33	(23–46)
	Senescence	47	(9–66)	14	(1–41)	11	(2–30)	91	(48–112)
Mc	G_{in}	6	(1–17)	7	(2–11)	7	(1–20)	7	(2–15)
(N = 8)	G_{max}	6	(1–16)	9	(1–13)	16	(7–52)	17	(7–30)
	G_{dec}	35	(13–55)	19	(7–69)	17	(3–65)	59	(4–93)
	G_{min}	4	(0–9)	5	(0–12)	6	(0–15)	12	(4–20)
	Greenup	12	(2–25)	9	(3–18)	11	(2–32)	21	(2–40)
	Senescence	36	(13–64)	21	(1–62)	19	(0–60)	71	(23–113)
Ds	G_{in}	15	(7–23)	17	(7–26)	12	(1–18)	12	(4–19)
(N = 6)	G_{max}	13	(4–25)	10	(0–26)	3	(2–8)	26	(17–38)
	G_{dec}	18	(0–45)	22	(1–42)	21	(4–49)	21	(4–48)
	G_{min}	9	(1–19)	17	(1–32)	19	(4–26)	8	(3–15)
	Greenup	29	(15–47)	27	(16–44)	14	(7–20)	38	(24–57)
	Senescence	23	(1–46)	36	(3–61)	29	(5–49)	20	(1–48)

absolute error (MAE) between the ExG_W and each of the MODIS VI based phenological metrics (Table 4). In general the MAE for metrics derived from EVI and MODIS phenology data are larger than those derived from NDVI and ExG_M data. Further, both the Dolly Sods and Smoky Look sites have slightly larger MAE values than the Bartlett Forest and Mammoth Cave sites. Given the rapid increase (spring) and decrease (autumn) in the ExG_W time series for both Smoky Look and Dolly Sods, this is expected because the 8-day temporal sampling of MODIS is not able to capture these rapid transitions. In contrast, dynamics in phenology at Mammoth Cave and Bartlett Forest data are more gradual, which leads to better fits, better correspondence between the different VI time series
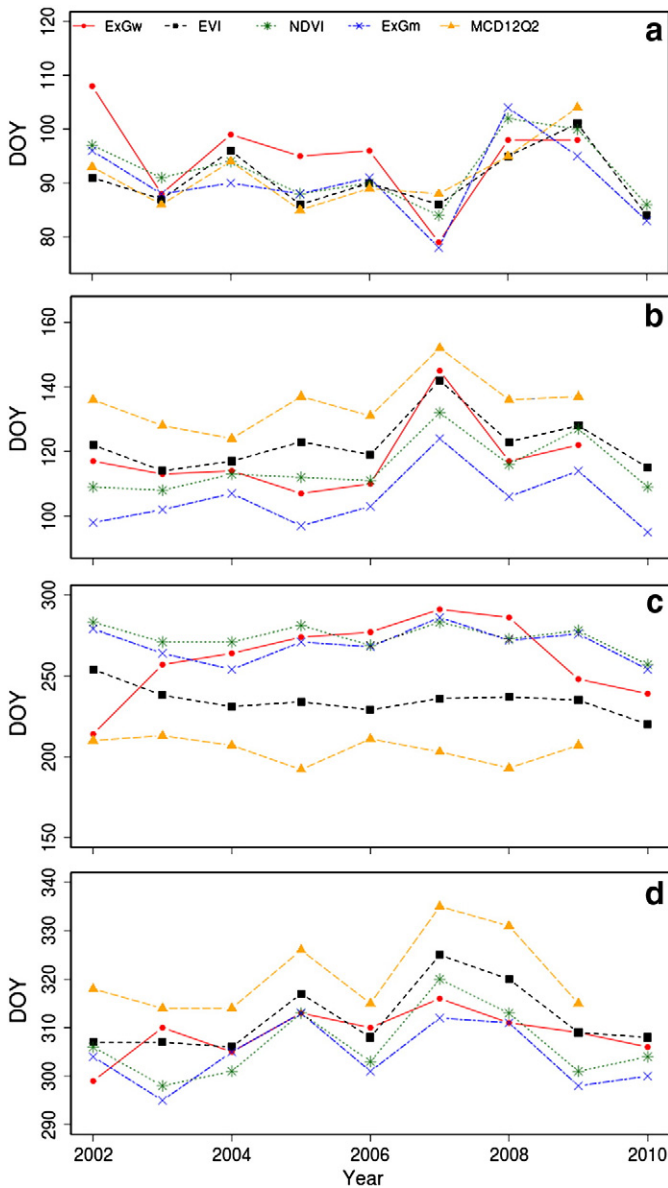

Fig. 5. a–d. Phenological indicators for the Mammoth Cave National Park (Mc) site covering the complete data series (2002–2009). Greenness increase (a), maximum (b), decrease (c) and minimum (d) for the ExG_W (red line, dot), MODIS EVI (black short dashed line, square), MODIS NDVI (green dotted line, star) and MODIS ExG_M (blue dotted dashed line, cross) are shown. All values were estimated using a logistic model estimated by non-linear least squares. For visual comparison values from the MODIS Land Cover Dynamics product (MCD12Q2) are also shown (orange long dashed line, triangle).

and the derived phenological indicators, and by extension, lower the MAE for both sites. (Table 4). It is interesting to note that MAE values at the Mammoth Cave site show relatively consistent patterns across metrics, the only exception being G_{dec}, which was influenced by missing data and/or outliers in 2009. When data from 2009 are excluded, MAE values are 4–9 and 6–16 for the NDVI and ExG_M based metrics (Table 4).

3.2. Interannual covariance among phenological indicators

Visual assessment of year-to-year covariation among phenological metrics suggests that VI data derived from MODIS and the cameras capture consistent patterns of interannual variation, presumably attributable to climate forcing (Fig. 5). For example, at the Mammoth Cave site, which has the longest time series of camera data, covariance among phenological indicators is visible in Fig. 5. In addition, the effects of early spring warming and a late frost event in 2007 are clearly evident (i.e., early onset of leaf growth, but delayed canopy maturity), and are consistent with previous work that documented pronounced vegetation response to unusual spring weather conditions in the central and eastern United States in 2007 (Gu et al., 2008).

More specifically, Spearman rank correlations among the various metrics (Table 5) vary significantly across sites. Smoky Look and Mammoth Cave are the only sites with large proportion of significant correlations between ExG_W and the MODIS VI based metrics; specifically, metrics derived from ExG_W were significantly correlated with the timing of increase across all MODIS phenology metrics (significant correlations ranging from $\rho = 0.59$ to 0.78, $p < 0.05$). Among the metrics derived from MODIS, those based on EVI for the timing of greenness maximum showed high positive and significant correlations with the webcam data for all but the Mammoth Cave site ($\rho = 0.9$, 0.85 and 0.79, $p < 0.05$ for Bartlett Forest, Smoky Look and Dolly Sods respectively). The timing of VI decrease for the Mammoth Cave site exhibited low to negative correlations with estimates based on ExG_W and MODIS VI data, suggesting especially high uncertainty in the estimated dates of this phenological metric. This result is consistent with the MAE values presented above. Because phenological metrics for both greenup and senescence values are derived from greenness increase and maximum or greenness decrease and minimum, respectively, negative correlation among phenological metrics will negatively influence test statistics. A consistent significant correlation is seen for greenness increase and minimum on the Smoky Look site; otherwise, the Dolly Sods site shows low covariance between estimated phenological indicators greenness decrease and minimum.

3.3. Dynamics in greenup and senescence

Comparison of phenological dynamics captured by the different VIs reveal that each VI and data source provides slightly different information related to canopy dynamics during leaf development and senescence. Fig. 3 illustrates different responses within and between sites, with rapid changes in both greenup and senescence captured by the ExG_W data at both Smoky Look and Dolly Sods, and more gradual changes at Mammoth Cave and Bartlett Forest. Temporal dynamics measured by the satellite data are more gradual. At all four sites MODIS EVI time series show evidence of asymmetry between and within spring and autumn periods. At the Bartlett Forest and Dolly Sods sites, spring canopy dynamics are relatively symmetric, with transitions located around the ~50th percentile and relatively low BR values of 0.55 and 0.11, respectively (Table 6). Also note the rapid development of the canopy at Bartlett Forest in 2010 due to exceptionally warm spring temperatures (Hufkens et al., 2011). Autumn dynamics are less symmetric and are positively biased, with BR values of 0.91, 1 and 0.83 at the Mammoth Cave, Dolly Sods and Smoky Look

Table 5
Spearman rank correlations between phenological indicator dates for DOY onset of greenness Increase, maximum, decrease, minimum (G_{in}, G_{max}, G_{dec} and G_{min} respectively), greenup and senescence periods for four different sites (Bartlett Experimental Forest, Bt; Look Rock in Smoky Look National Park, Sl; Mammoth Cave National Park, Mc and Dolly Sods Wilderness, Ds). Statistically significant values (p<0.05) are denoted with *.

	Index	Increase	Maximum	Decrease	Minimum	Greenup	Senescence
Bt	EVI	0.67	0.90*	−0.15	0.46	0.76	−0.60
(N=5)	NDVI	0.34	0.56	0.70	0.57	0.41	0.90*
	ExG_m	0.23	0.50	0.30	0.92	0.00	0.30
	MCD12Q2	0.26	0.80	0.00	0.74	−0.33	−0.26
Sl	EVI	0.74*	0.85*	0.49	0.87*	0.59*	0.22
(N=10)	NDVI	0.72*	0.68*	0.40	0.85*	0.43	−0.33
	ExG_m	0.59*	0.35	0.90*	0.83*	−0.10	0.61*
	MCD12Q2	0.71*	0.56	−0.09	0.87*	0.38	0.03
Mc	EVI	0.77*	0.62	−0.07	0.82*	−0.16	−0.58
(N=9)	NDVI	0.73*	0.67*	0.13	0.54	0.45	−0.51
	ExG_m	0.78*	0.76*	0.23	0.49	0.72	−0.18
	MCD12Q2	0.68*	0.47	−0.48	0.65	−0.05	−0.45
Ds	EVI	−0.28	0.78*	0.19	0.36	0.70*	0.04
(N=7)	NDVI	0.74*	0.16	0.21	−0.39	−0.31	0.20
	ExG_m	0.83*	0.80*	0.07	−0.36	0.39	−0.02
	MCD12Q2	0.76	−0.09	0.52	0.27	−0.38	0.14

sites, respectively. Bartlett Forest has a BR of −0.48, which suggests a negative bias in the satellite-based model fits compared to the webcam date (Fig. 6a, top panel). The autumn BR value of Smoky Look is approximately 1, suggesting that some of the differences among the logistic fits are associated with different phases between model fits. This interpretation is confirmed by visual inspection of the VI profiles (Fig. 6c) and was consistent throughout.

Dynamics in NDVI show positive bias for all sites in spring (Table 6), with BR values close to 1.0 for the Bartlett, Smoky Look, and Mammoth Cave sites. Positive values indicate earlier increase in VI relative to the timing of increase in ExG_w from webcam data. Moreover, for those sites with BR values close or equal to 1, the logistic fit based on MODIS NDVI data consistently reaches its maximum before that of ExG_W, which suggests that the main difference that is associated in the time series is related to a phase shift rather than a difference in slope. BR values in autumn are negative for Bartlett and Mammoth Cave (Fig. 6a–c, center panel). In contrast, both Dolly Sods and Smoky Looks sites exhibited positive BR values in the autumn (Fig. 6b–d, center panel). The more condensed plots along the 5 percent increments suggest a faster development of NDVI compared to the autumn results of EVI (Fig. 6, autumn top and center panels) and corroborated by visual interpretation of Fig. 3.

For ExG_M, we note that both Smoky Look and Dolly Sods show similar patterns with large positive BR values in both spring and autumn. This result is the product of earlier onset in the timing of VI decrease and minimum at the Smoky Look and Dolly Sods sites for ExG_M (G_{dec} DOY 276 and 234; G_{min} DOY 304 and 284) relative to those from ExG_W (G_{dec} DOY 287 and 241; G_{min} DOY 306 and 303). The timing of

ExG_M for Bartlett Forest and Mammoth Cave is slightly different, with a large positive bias during spring and negative bias during autumn. This pattern is reflected in the mean values for Gin, G_{max}, G_{dec}, G_{min} and both greenup and senescence periods in Table 3. Similar to the NDVI autumn results a fast development of ExG_M compared to the values as estimated for EVI during autumn is recorded for all sites.

4. Discussion

Several recent studies have successfully linked near-surface remote sensing data to canopy flux measurements (Graham et al., 2006; Jenkins et al., 2007; Richardson et al., 2007, 2009). At coarser spatial scales satellite remote sensing has been used for over two decades to study and monitor ecosystem properties, phenology and fluxes. In this study, we assessed if and how phenological time series and metrics derived from near-surface remote sensing compare to those derived from satellite remote sensing. Our results suggest that while there is clear correlation between near surface and satellite remote sensing quantities, the relationship depends on a number of different factors.

Recent work has shown that RGB camera images acquired during high illumination clear-sky conditions provide the best basis for monitoring canopy phenology (Sonnentag et al., 2012). Based on this result, we developed a moving-window technique that effectively smoothed the web camera time series data and removed variance associated with illumination conditions. The more data that are available within each window (i.e., the more images acquired each day), the more reliable the results tend to be (Fig. 3a–c). Because sampling frequency influences the efficacy of this method, results will vary from site to site, depending on the sampling frequency of image acquisition.

Differences among estimates of phenological metrics and the quality of logistic fits can be attributed to differences in seasonal dynamics in phenology captured by the different VIs (Fig. 2). Phenological metrics based on logistic model fits tend to bias estimates for timing in the spring onset in VI increase from MODIS data early relative to the camera data, which is consistent with previous results from other studies that have used MODIS products (Jenkins et al., 2007; Soudani et al., 2008; Turner et al., 2005, 2006). Several factors have been previously suggested to explain this pattern, including early understory development (Ahl et al., 2006; Schwartz et al.,

Table 6
Bias ratios (BR) quantifying the nature and magnitude of bias in logistic fits based on the satellite VI's relative to logistic fits based on the ExG_W data. The value of this metric indicates whether model fits to the satellite VIs are positively biased (~1), negatively biased (~−1) or display a more complex pattern including a change in steepness relative to the ExG_W data.

	Bartlett		Dolly Sods		Look Rock		Mammoth Cave	
	Spring	Fall	Spring	Fall	Spring	Fall	Spring	Fall
EVI	0.55	−0.48	0.11	1	0.84	0.83	−0.36	0.91
NDVI	1	−0.98	0.46	0.16	1	1	1	−0.90
ExG_M	1	−0.91	0.98	1	1	1	1	−0.39

2002), spatial integration over areas with significant topography (Fisher et al., 2007), and snow melt (Delbart et al., 2006). This latter issue causes NDVI and EVI values to increase, leading to spurious estimates for the timing of canopy development (Delbart et al., 2006; Kobayashi et al., 2007). In this study, we limited the influence of snow by screening and removing snow-contaminated MODIS data. More importantly, the large FOV of satellite-based sensors such as MODIS integrate surface reflectances over substantially larger areas than those measured by near-surface remote sensing cameras, which confounds the comparison. Further, the temporal resolution of the MODIS products (8-day) used here, which is dictated by the frequency of missing data caused by clouds in many parts of the world, does not support precise characterization of phenology in canopies characterized by rapid leaf emergence and development during spring (Ahl et al., 2006). As a consequence, it is not realistic to expect MODIS data to exactly replicate data from cameras.

Results from this work show that comparisons of near surface and satellite remote sensing-based estimates of phenology are affected by the bands used to compute VIs from each data source. Although some patterns were consistent for MODIS relative to results from the cameras (e.g., earlier spring increase in VIs), seasonal dynamics among the various MODIS VIs were often markedly different. The different responses of EVI and NDVI to increasing leaf area

index (LAI) is well-documented (Huete et al., 2002). Similarly, NDVI is known to saturate before the EVI, which contributes to differences in their seasonal profiles. As a consequence, the seasonal profile of EVI tends to be less steep than NDVI during spring, with maximum values occurring later compared to both the NDVI and ExG_M. Differences in the slope of EVI-based logistic fits and resulting patterns in the timing of VI increase and VI maximum were consistent across all sites (Fig. 6a–d top panel). Because the slope of logistic fits based on ExG_W, ExG_M and EVI tend to be lower than those for NDVI, estimates for phenophase transition dates based on these VIs differ from those estimated using NDVI data because the transitions are much more gradual. Consistent with the results of Fisher et al. (2007), correlation in temporal dynamics between MODIS EVI and ExG_W was highest at roughly 50% of the seasonal amplitude in each VI. Unfortunately, the ecological meaning of this metric ("half-maximum greenness") is unclear, and so the utility of this result is uncertain.

Comparison of autumn phenological metrics estimated from MODIS data with metrics based on ExG_W data showed similar patterns to those in spring. The slow rate of change (low slope) in autumn VI data produced early estimates for G_{dec} and late estimates for G_{min} in metrics based on MODIS data relative comparable estimates from the camera data. Distinct differences were also noted in the timing of NDVI dynamics among sites. Specifically, NDVI values
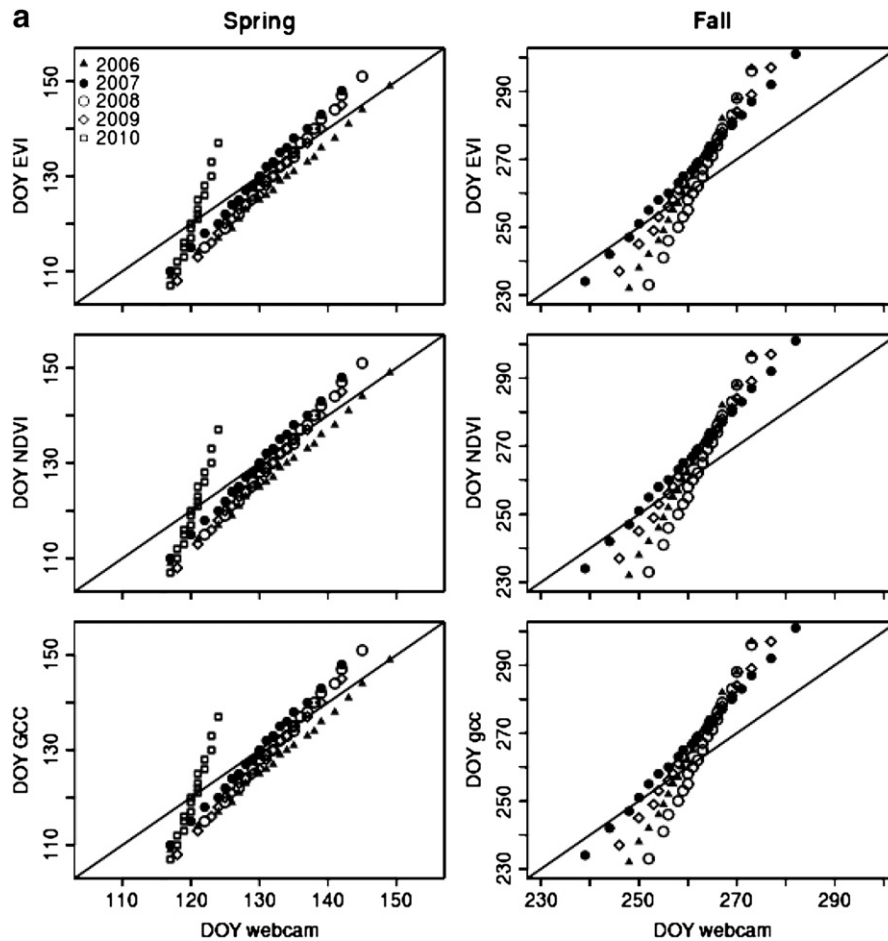

Fig. 6. a–d. Deviation between the logistic fits for satellite data (VI) relative to the digital camera data (ExG_W) at 5 percent increments in the amplitude of each fit from 5 to 95%. The y-axis denotes the satellite based estimates (DOY), x-axis denotes the ExG_W based estimates (DOY) both at 5 percent increments between 5 and 95%. Different years are plotted using different characters with an open triangle, plus sign, x, asterisk, black square, black triangle, black circle, open circle, open diamond and an open square for years 2001 to 2010 respectively. Data is presented for the four sites of interest (Bartlett Experimental Forest, Look Rock in Smoky Look National Park; Mammoth Cave National Park and Dolly Sods Wilderness).
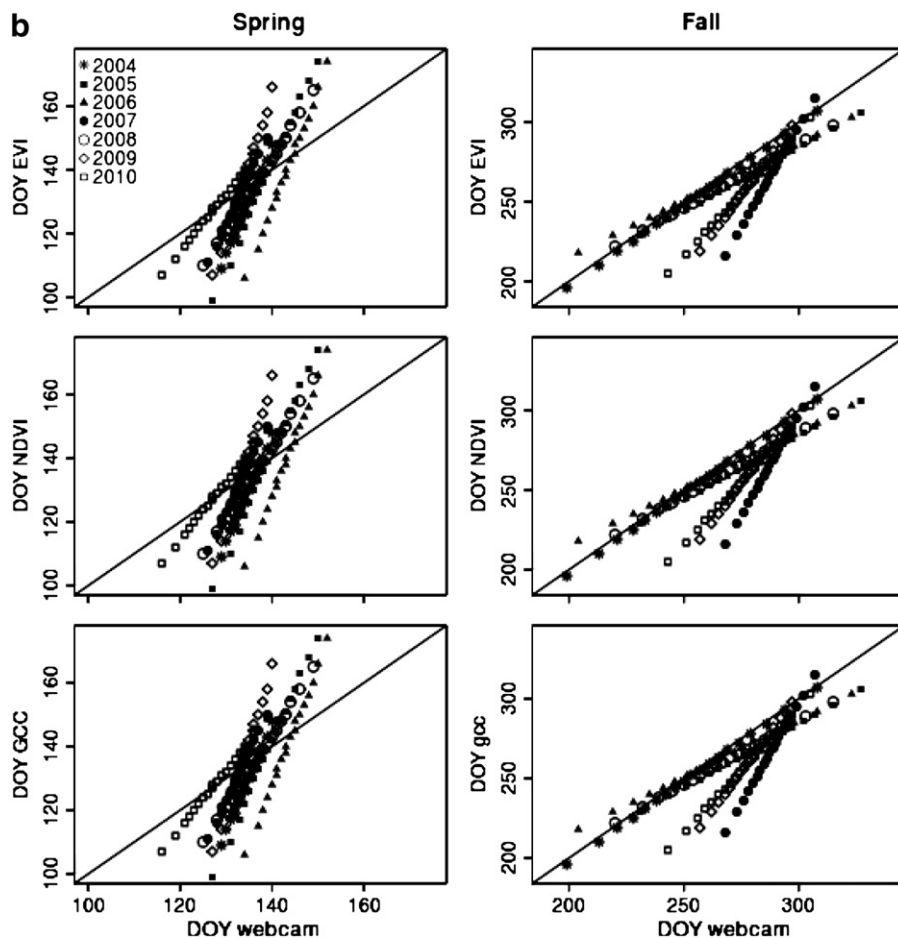
Fig. 6 (*continued*).

tended to start decreasing earlier at both Dolly Sods and Smoky Look, but later at Bartlett Forest and Mammoth Cave. This site-to-site variability is explained by the slow rate of VI decrease in the autumn. Because the rate of change in VI tends to be more gradual in autumn, estimates of phenological metrics is more challenging relative to spring.

The degree to which interannual variation in phenology is detectable from satellite remote sensing is a central methodological question in phenology research. Although visual inspection of phenological metrics suggests year-to-year correlations, statistical covariance between metrics estimated from ExG_W data and those retrieved from MODIS VI data was relatively weak. In particular, interannual covariance in the estimated timing of VI increase and minimum was statistically significant only at the Mammoth Cave site. Phenological metrics at the other sites showed either no covariation or weak covariation. A key factor that influences these results is the length of time series at each site. Specifically, because the time series are quite short, it is not surprising that the statistical significance of results is low (critical values for $N = 5$ at $p = 0.05$, 0.01, 0.001 are 0.878, 0.959, 0.991 respectively). The results for the Mammoth Cave site, which provided the longest time series in the PhenoCam archive, support this inference.

A confounding factor, which probably contributes to these results, is that variability in phenological characteristics within the ROI of individual cameras has been shown to influence estimations of phenophase transitions by up to a week (Richardson et al., 2009). The camera ROI at Mammoth Cave is quite large, and provides good representation of landscape-scale phenological dynamics

and less variance introduced by species-specific phenology. Conversely, the smaller ROI at the other sites may explain the relatively low covariance between the satellite and camera data, because VIs extracted from these images reflect a small set of individual trees, but not the phenology of the larger landscape. In this context it is important to note that phenological dynamics in the autumn can vary substantially across species, with differences in transition dates as large as two weeks within the same ROI (Richardson et al., 2009). In this work, we found that the smaller ROI at Dolly Sods and Smoky Look significantly influenced autumn ExG_W values. The ROIs for both these sites had fewer trees relative to the ROIs for Bartlett and Mammoth Cave, and were therefore more sensitive to species-specific phenological dynamics within the camera ROIs. These results suggest that the camera field of view and ROI used for analysis can significantly influence the character of camera VI time series, and that in order for data from cameras to be used as a basis for calibration and validation of satellite-derived phenology products, it is critical for the camera FOV to include a representative sample of the landscape and not simply focus on a few individual trees.

5. Conclusions

As described by Richardson et al. (2010) and Fisher et al. (2007), two research paradigms are currently being pursued within the phenology science community. One paradigm uses ground observations; the other uses satellite-based observations. Ground observations have the advantage of being able to provide information related to
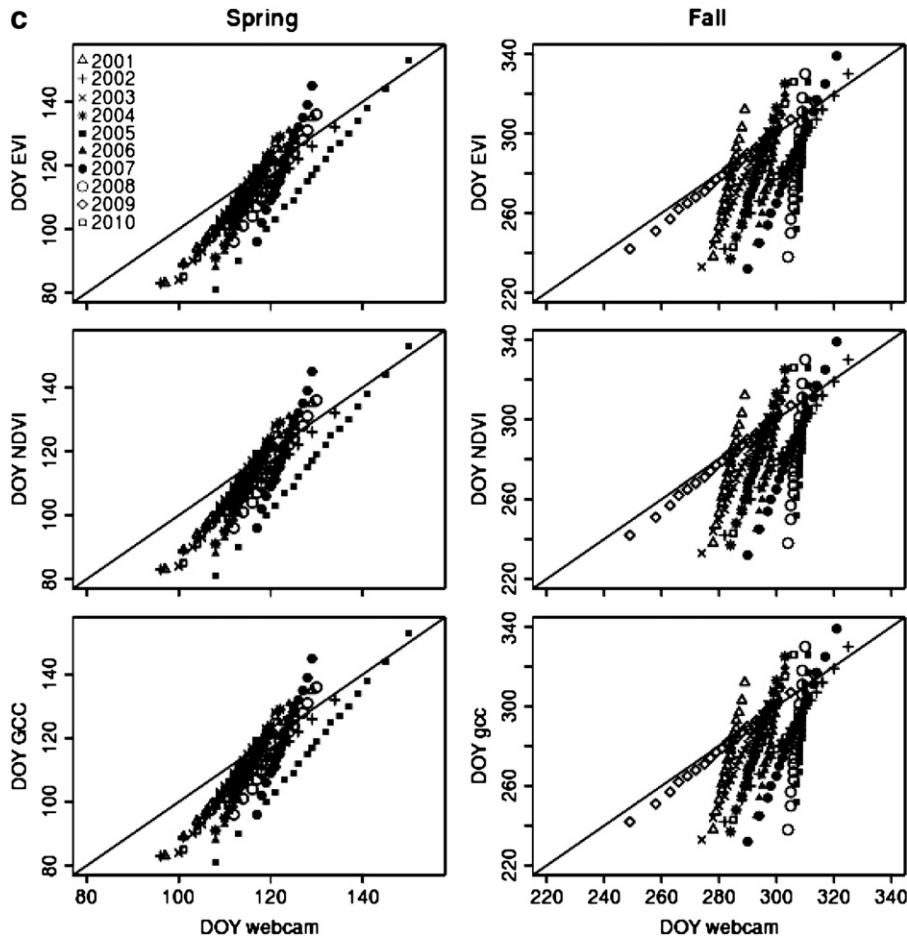
Fig. 6 (*continued*).

specific plants and species, but are subjective, labor intensive, and difficult to extrapolate over large scales. Satellite observations, on the other hand, provide synoptic to global coverage at coarser spatial and temporal resolutions. In this context, near-surface phenology measurements derived from commercial cameras have emerged as a valuable tool for characterizing phenology at local scales.

While the results from our study provide significant support for future efforts linking satellite and near-surface remote sensing, our analysis also reveals that substantial care must be devoted to ensure that camera VIs and ROIs are representative of and comparable to satellite-derived data. Specifically, results from our study show significant agreement between phenological time series and metrics derived from these two data sources. However, issues of scale and representation in near-surface remote sensing data can significantly affect measurements, and specifically, the degree to which camera data are representative of the larger landscape is highly dependent on the camera FOV. To help account for and characterize small-scale variability within and outside of the camera FOV, high resolution satellite imagery could be used to better understand how representative camera ROIs are relative to satellite sensor FOV (e.g., Baccini et al., 2007; Morisette et al., 2002). Further, our results show that the specific VI used to monitor phenology exerts substantial influence on satellite derived VI time series (and associated phenological metrics), and by extension, how they compare to VI time series and metrics obtained from near-surface remote sensing. As a result, not all near-surface remote sensing camera data will be suitable for comparison or fusion with satellite data. The work presented in this paper helps to bridge the divide between near-surface and satellite remote sensing. However, more work is required to develop formal protocols for evaluating, calibrating and validating satellite remote sensing phenology products using near surface remote sensing at a regional to continental scale.

Acknowledgments

References

Ahl, D. E., Gower, S. T., Burrows, S. N., Shabanov, N. V., Myneni, R. B., & Knyazikhin, Y. (2006). Monitoring spring canopy phenology of a deciduous broadleaf forest using MODIS. *Remote Sensing of Environment, 104*, 88–95.

Ahrends, H. E., Brügger, R., Stöckli, R., Schenk, J., Michna, P., Jeanneret, F., et al. (2008). Quantitative phenological observations of a mixed beech forest in
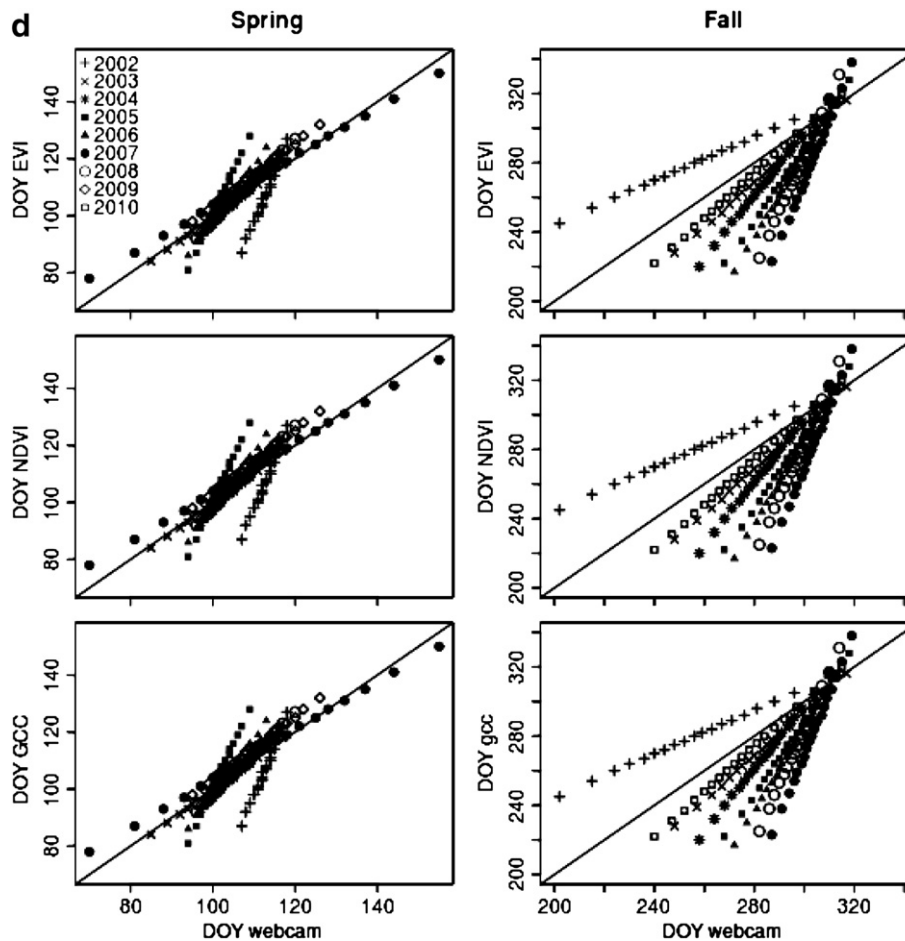
Fig. 6 (*continued*).

northern Switzerland with digital photography. *Journal of Geophysical Research*, *113*, G04004.

Ahrends, H. E., Brügger, R., Stöckli, R., Schenk, J., Michna, P., Jeanneret, F., et al. (2008). Quantitative phenological observations of a mixed beech forest in northern Switzerland with digital photography. *Journal of Geophysical Research*, *113*, G04004.

Ahrends, H. E., Etzold, S., Kutsch, W. L., Stoeckli, R., Bruegger, R., Jeanneret, F., et al. (2009). Tree phenology and carbon dioxide fluxes: Use of digital photography for process-based interpretation at the ecosystem scale. *Climate Research*, *39*, 261–274.

Baccini, A., Friedl, M. A., Woodcock, C. E., & Zhu, Z. (2007). Scaling field data to calibrate and validate moderate spatial resolution remote sensing models. *Photogrammetric Engineering and Remote Sensing*, *73*, 945–954.

Badeck, F. -W., Bondeau, A., Bôttcher, K., Doktor, D., Lucht, W., Schaber, J. r., et al. (2004). Responses of spring phenology to climate change. *New Phytologist*, *162*, 295–309.

Baldocchi, D. D., Black, T. A., Curtis, P. S., Falge, E., Fuentes, J. D., Granier, A., et al. (2005). Predicting the onset of net carbon uptake by deciduous forests with soil temperature and climate data: A synthesis of FLUXNET data. *International Journal of Biometeorology*, *49*, 377–387.

Betancourt, J. L., Schwartz, M. D., Breshears, D. D., Brewer, C. A., Frazer, G., Gross, J. E., et al. (2007). Evolving plans for the USA National Phenology Network. *EOS Earth Observer*, *88*, 211.

Bogaert, J., Zhou, L., Tucker, C. J., Myneni, R. B., & Ceulemans, R. (2002). Evidence for a persistent and extensive greening trend in Eurasia inferred from satellite vegetation index data. *Journal of Geophysical Research*, *107*(D11).

Chuine, I., Cambon, G., & Comtois, P. (2000). Scaling phenology from the local to the regional level: Advances from species-specific phenological models. *Global Change Biology*, *6*, 943–952.

Chuine, I., Yiou, P., Viovy, N., Seguin, B., Daux, V., & Ladurie, E. L. R. (2004). Historical phenology: Grape ripening as a past climate indicator. *Nature*, *432*, 289–290.

Churkina, G., Schimel, D., Braswell, B. H., & Xiao, X. (2005). Spatial analysis of growing season length control over net ecosystem exchange. *Global Change Biology*, *11*, 1777–1787.

Cleland, E. E., Chuine, I., Menzel, A., Mooney, H. A., & Schwartz, M. D. (2007). Shifting plant phenology in response to global change. *Trends in Ecology & Evolution*, *22*, 357–365.

Delbart, N., Le Toan, T., Kergoat, L., & Fedotova, V. (2006). Remote sensing of spring phenology in boreal regions: A free of snow-effect method using NOAA-AVHRR and SPOT-VGT data (1982–2004). *Remote Sensing of Environment*, *101*, 52–62.

Fisher, Jeremy Isaac, Mustard, J. F., & Vadeboncoeur, M. A. (2006). Green leaf phenology at Landsat resolution: Scaling from the field to the satellite. *Remote Sensing of Environment*, *100*, 265–279.

Fisher, Jeremy I., Richardson, A. D., & Mustard, J. F. (2007). Phenology model from surface meteorology does not capture satellite-based greenup estimations. *Global Change Biology*, *13*, 707–721.

Fitter, A. H., & Fitter, R. S. R. (2002). Rapid changes in flowering time in British plants. *Science*, *296*, 1689–1691.

Friedl, M. A., Sulla-Menashe, D., Tan, B., Schneider, A., Ramankutty, N., Sibley, A., et al. (2010). MODIS Collection 5 global land cover: Algorithm refinements and characterization of new datasets. *Remote Sensing of Environment*, *114*, 168–182.

Fry, J., Xian, G., Jin, S., Dewitz, J., Homer, C., Yang, L., et al. (2011). Completion of the 2006 National Land Cover Database for the conterminous United States. *PE&RS*, *77*, 858–864.

Ganguly, S., Friedl, M. A., Tan, B., Zhang, X. Y., & Verma, M. (2010). Land surface phenology from MODIS: Characterization of the Collection 5 global land cover dynamics product. *Remote Sensing of Environment*, *114*, 1805–1816.

Graham, E. A., Hamilton, M. P., Mishler, B. D., Rundel, P. W., & Hansen, M. H. (2006). *Use of a Networked Digital Camera to Estimate Net CO₂ Uptake of a Desiccation-Tolerant Moss.* : University of Chicago Press.

Graham, E. A., Riordan, E. C., Yuen, E. M., Estrin, D., & Rundel, P. W. (2010). Public internet-connected cameras used as a cross-continental ground-based plant phenology monitoring system. *Global Change Biology*, *16*, 3014–3023.

Graham, E. A., Yuen, E. M., Robertson, G. F., Kaiser, W. J., Hamilton, M. P., & Rundel, P. W. (2009). Budburst and leaf area expansion measured with a novel mobile camera system and simple color thresholding. *Environmental and Experimental Botany*, *65*, 238–244.

Gu, L., Hanson, P. J., Post, W. M., Kaiser, D. P., Yang, B., Nemani, R., et al. (2008). The 2007 eastern US spring freeze: Increased cold damage in a warming world. *BioScience*, *58*, 253–262.

Hollinger, D. Y., Goltz, S. M., Davidson, E. A., Lee, J. T., Tu, K., & Valentine, H. T. (1999). Seasonal patterns and environmental control of carbon dioxide and water vapour exchange in an ecotonal boreal forest. *Global Change Biology*, *5*, 891–902.

Huete, A., Didan, K., Miura, T., Rodriguez, E. P., Gao, X., & Ferreira, L. G. (2002). Overview of the radiometric and biophysical performance of the MODIS vegetation indices. *Remote Sensing of Environment*, *83*, 195–213.

Hufkens, K., Sonnentag, O., Keenan, K., Richardson, D. A., Melaas, E., Bailey, A., et al. (2011). *Community impacts of a mid-May frost event during an anomalously warm spring. PhenoAlp final project meeting, 12–14 October.* Torgnon, Italy.

Jacobs, N., Burgin, W., Fridrich, N., Abrams, A., Miskell, K., Braswell, R., et al. (2009). The global network of outdoor webcams: Properties and applications. *ACM International Conference on Advances in Geographic Information Systems* (pp. 111–120).

Jenkins, J. P., Richardson, A. D., Braswell, B. H., Ollinger, S. V., Hollinger, D. Y., & Smith, M. L. (2007). Refining light-use efficiency calculations for a deciduous forest canopy using simultaneous tower-based carbon flux and radiometric measurements. *Agricultural and Forest Meteorology*, *143*, 64–79.

Keeling, C. D., Chin, J. F. S., & Whorf, T. P. (1996). Increased activity of northern vegetation inferred from atmospheric CO_2 measurements. *Nature*, *382*, 146–149.

Kemp, P. R. (1983). Phenological patterns of Chihuahuan Desert plants in relation to the timing of water availability. *Journal of Ecology*, *71*, 427–436.

Kobayashi, H., Suzuki, R., & Kobayashi, S. (2007). Reflectance seasonality and its relation to the canopy leaf area index in an eastern Siberian larch forest: Multi-satellite data and radiative transfer analyses. *Remote Sensing of Environment*, *106*, 238–252.

Menzel, A. (2002). Phenology: Its importance to the global change community — An editorial comment. *Climatic Change*, *54*, 379–385.

Menzel, A., Sparks, T. H., Estrella, N., Koch, E., Aasa, A., Ahas, R., et al. (2006). European phenological response to climate change matches the warming pattern. *Global Change Biology*, *12*, 1969–1976.

Morisette, J. T., Privette, J. L., & Justice, C. O. (2002). A framework for the validation of MODIS Land products. *Remote Sensing of Environment*, *83*, 77–96.

Morisette, J. T., Richardson, A. D., Knapp, A. K., Fisher, J. I., Graham, E. A., Abatzoglou, J., et al. (2008). Tracking the rhythm of the seasons in the face of global change: Phenological research in the 21st century. *Frontiers in Ecology and the Environment*, *7*, 253–260.

Myneni, R. B., Keeling, C. D., Tucker, C. J., Asrar, G., & Nemani, R. R. (1997). Increased plant growth in the northern high latitudes from 1981 to 1991. *Nature*, *386*, 698–702.

Nemani, R. R., Keeling, C. D., Hashimoto, H., Jolly, W. M., Piper, S. C., Tucker, C. J., et al. (2003). Climate-driven increases in global terrestrial net primary production from 1982 to 1999. *Science*, *300*, 1560–1563.

Parmesan, C. (2007). Influences of species, latitudes and methodologies on estimates of phenological response to global warming. *Global Change Biology*, *13*, 1860–1872.

Parmesan, C., & Yohe, G. (2003). A globally coherent fingerprint of climate change impacts across natural systems. *Nature*, *421*, 37–42.

Penuelas, J., Filella, I., & Comas, P. (2002). Changed plant and animal life cycles from 1952 to 2000 in the Mediterranean region. *Global Change Biology*, *8*, 531–544.

Richardson, A. D., Andy Black, T., Ciais, P., Delbart, N., Friedl, M. A., Gobron, N., et al. (2010). Influence of spring and autumn phenological transitions on forest ecosystem productivity. *Philosophical Transactions of the Royal Society B: Biological Sciences*, *365*, 3227–3246.

Richardson, A. D., Bailey, A. S., Denny, E. G., Martin, C. W., & O'Keefe, J. (2006). Phenology of a northern hardwood forest canopy. *Global Change Biology*, *12*, 1174–1188.

Richardson, A. D., Braswell, B. H., Hollinger, D. Y., Jenkins, J. P., & Ollinger, S. V. (2009). Near-surface remote sensing of spatial and temporal variation in canopy phenology. *Ecological Applications*, *19*, 1417–1428.

Richardson, A., Jenkins, J., Braswell, B., Hollinger, D., Ollinger, S., & Smith, M. -L. (2007). Use of digital webcam images to track spring green-up in a deciduous broadleaf forest. *Oecologia*, *152*, 323–334.

Sakai, R. K., Fitzjarrald, D. R., & Moore, K. E. (1997). Detecting leaf area and surface resistance during transition seasons. *Agricultural and Forest Meteorology*, *84*, 273–284.

Schaaf, C. B., Gao, F., Strahler, A. H., Lucht, W., Li, X., Tsang, T., et al. (2002). First operational BRDF, albedo nadir reflectance products from MODIS. *Remote Sensing of Environment*, *83*, 135–148.

Schwartz, M. D., Ahas, R., & Aasa, A. (2006). Onset of spring starting earlier across the Northern Hemisphere. *Global Change Biology*, *12*, 343–351.

Schwartz, M. D., & Hanes, J. M. (2010). Intercomparing multiple measures of the onset of spring in eastern North America. *International Journal of Climatology*, *30*, 1614–1626.

Schwartz, M. D., Reed, B. C., & White, M. A. (2002). Assessing satellite-derived start-of-season measures in the conterminous USA. *International Journal of Climatology*, *22*, 1793–1805.

Sonnentag, O., Hufkens, K., Teshera-Sterne, C., Young, A. M., Friedl, M., Braswell, B. H., et al. (2012). Digital repeat photography for phenological research in forest ecosystems. *Agricultural and Forest Meteorology*, *22*, 152.

Soudani, K., le Maire, G., Dufrine, E., Francois, C., Delpierre, N., Ulrich, E., et al. (2008). Evaluation of the onset of green-up in temperate deciduous broadleaf forests derived from Moderate Resolution Imaging Spectroradiometer (MODIS) data. *Remote Sensing of Environment*, *112*, 2643–2655.

Sparks, T. H., & Menzel, A. (2002). Observed changes in seasons: An overview. *International Journal of Climatology*, *22*, 1715–1725.

Spearman, C. (1904). The proof and measurement of association between two things. *American Journal of Psychology*, *15*, 72–101.

Tucker, C. J. (1979). Red and photographic infrared linear combinations for monitoring vegetation. *Remote Sensing of Environment*, *8*, 127–150.

Turner, D. P., Ritts, W. D., Cohen, W. B., Gower, S. T., Running, S. W., Zhao, M., et al. (2006). Evaluation of MODIS NPP and GPP products across multiple biomes. *Remote Sensing of Environment*, *102*, 282–292.

Turner, D. P., Ritts, W. D., Cohen, W. B., Maeirsperger, T. K., Gower, S. T., Kirschbaum, A. A., et al. (2005). Site-level evaluation of satellite-based global terrestrial gross primary production and net primary production monitoring. *Global Change Biology*, *11*, 666–684.

White, M. A., de Beurs, K. M., Didan, K., Inouye, D. W., Richardson, A. D., Jensen, O. P., et al. (2009). Intercomparison, interpretation, and assessment of spring phenology in North America estimated from remote sensing for 1982–2006. *Global Change Biology*, *15*, 2335–2359.

Wingate, L., Richardson, A., Weltzin, J. F., Nasahara, K. N., & Grace, J. (2008). Keeping an eye on the carbon balance: Linking canopy development and net ecosystem exchange using a webcam. *Fluxletter*, *1*(2), 14–17.

Woebbecke, D. M., Meyer, G. E., Vonbargen, K., & Mortensen, D. A. (1995). Color indexes for weed identification under various soil, residue, and lighting conditions. *Transactions of the Asae*, *38*, 259–269.

Zhang, X., Friedl, M. A., Schaaf, C. B., Strahler, A. H., Hodges, J. C. F., Gao, F., et al. (2003). Monitoring vegetation phenology using MODIS. *Remote Sensing of Environment*, *84*, 471–475.

Zhang, X., Tarpley, D., & Sullivan, J. T. (2007). Diverse responses of vegetation phenology to a warming climate. *Geophysical Research Letters*, *34*, L19405.

Zhang, Q., Xiao, X., Braswell, B., Linder, E., Ollinger, S., Smith, M. -L., et al. (2006). Characterization of seasonal variation of forest canopy in a temperate deciduous broadleaf forest, using daily MODIS data. *Remote Sensing of Environment*, *105*, 189–203.